TUNABLE POLY(URETHANE-UREA) BASED ALIGNED CARBON-NANOTUBE POLYMER NANOCOMPOSITES

Jeffrey L. Gair Jr.[1,2,3], Robert H. Lambeth[4], Daniel P. Cole[1], Dale L. Lidston[3], Alex J. Hsieh[4], Hugh A. Bruck[2], Mark L. Bundy[1], Brian L. Wardle[3]

[1]U.S. Army Research Laboratory, RDRL-VTM, Aberdeen Proving Ground, MD 21005, USA
[2]Department of Mechanical Engineering, University of Maryland, College Park, MD 20742, USA
[3]Department of Aeronautics and Astronautics, Massachusetts Institute of Technology, Cambridge, MA 02139, USA
[4]U.S. Army Research Laboratory, RDRL-WMM, Aberdeen Proving Ground, MD 21005, USA

Keywords: Polymer Nanocomposites, Carbon Nanotubes, Polyurethan-urea, Crystallization

ABSTRACT

A novel process for synthesizing poly(urethane-urea) (PUU) based vertically-aligned carbon-nanotubes (CNTs) has been demonstrated. This method employs the use of blocked diisocyanate which permits thermally-controlled polymerization. The resulting polymer nanocomposites (PNCs) had a 1% V_f of CNTs with consistent alignment and dispersion, following the morphology of the as-grown CNTs. Thermal analysis revealed that the presence of CNTs induced hard-segment crystallization in the PUU matrix, which in turn stabilized thermal degradation of the hard-segments. It was also found that increasing hard-segment content resulted in reduced chain mobility, leading to greater phase-mixing of the in-situ polymerized PUU matrix. CNTs were found to increase modulus by up to 650MPa, offering an improvement of over 350% over the neat PUU matrix.

1 INTRODUCTION

The aerospace industry is constantly seeking to improve the range and effectiveness of their vehicles; whether via lightweighting [1], fatigue resistance [2]–[4], or corrosion resistance [5], [6]. Metals are particularly susceptible to cyclical effects, which have been found to account for 86% of all helicopter material failures [3]. In addition to this, corrosion repairs cost the USAF ~$1.47 billion in 2004, a number which had grown by 60% since 1990 [7].

Composites have been investigated significantly, though they too have weaknesses. While exhibiting excellent properties under fiber-dominated loading, these materials upon exposure to matrix-dominated loading conditions often lead to failure in matrix-rich regions [4], [8], [9]. To circumvent this issue, nanoscale fillers have been used to reinforce the matrix-rich regions [10]–[12], though with varying efficacy. In many cases, dispersion and alignment issues reduce the enhancements offered by the nanofillers, and can even reduce mechanical properties in regions of aggregation. One means of overcoming this issue is to grow the CNTs directly on the surface of the fibers, which has been shown to produce excellent dispersion and alignment [13]. These CNTs have been found to reinforce the matrix significantly, providing both interlaminar and intralaminar reinforcement [14].

The complexity of these hierarchical composite systems, however, can make understanding the fundamental science governing the interaction of matrix and CNTs difficult. This could potentially confound the data and make accurate interpretation impossible. Polymer nanocomposites (PNCs) comprising vertically-aligned CNTs and matrix material have been selected as a suitable platform for understanding the phenomena at play between the CNTs and the matrix [15]. By performing thermal and nanoscale mechanical characterization, a glimpse into these fundamental interactions can be made.

Polyurethane-urea (PUU) has been of considerable interest due to its mechanical and thermal tunability [16]. By altering the stoichiometric ratios of diamine to polyol, stiffness can be tuned, while adjusting polyol molecular weight affects phase-mixing and rate-sensitivity [17], [18]. The degree of

control in mechanical properties makes fundamental research in this are extremely attractive. Combining these materials with CNTs, and eventually incorporating them into hierarchical composites is of particular interest to the development of new aerospace materials.

2 METHODS

2.1 Matrix Synthesis

In order to circumvent the problems associated with infusing PUU into vertically-aligned CNT forests, a stoveable PUU was necessary. To accomplish this, a blocked-HMDI (Desmodur BL5375, Cavestro) was used; the blocking groups are released with heat. This was combined in the requisite stoichiometric ratios with DETA (Ethacure 100-LC, Albemarle), PTMO (PolyTHF 650, BASF), and tin catalyst (DBTL). Two stoichiometric varieties were fabricated: at 2:1:1 ratio of HMDI:DETA:PTMO (PUU211) and a 5:4:1 ratio of HMDI:DETA:PTMO (PUU541). The materials were weighed and then mixed for 5min. using an over-head stirrer. The prepolymer was then degassed for 1hr. to remove any bubbles which had formed during the mixing process. Neat polymer materials were formed by pouring the degassed PUU prepolymer into molds.

In order to ensure complete cure of the PUU without introducing thermal damage, a relatively slow, low-temperature cure was selected for PUU synthesis. Based on the manufacturer recommendations and the known properties of the constituent materials, 130°C was chosen as the cure temperature. Materials were allowed to cure at this temperature for 24hrs, which produced stable and undegraded PUU polymers. The PUU was cured in a nitrogen purge in order to minimize oxidation of the amine.

2.2 Polymer Nanocomposite Fabrication

Preparation of polymer nanocomposites (PNCs) began with the growth of vertically-aligned CNT forests via methods developed previously [15]. These forests were then delaminated from the silicon wafers on which they were grown, and placed in silicone molds. The mixed and degassed PUU prepolymer was then poured over the forests until saturated. To aid in wetting, the molds containing the forests and prepolymer were placed in an oven set to 80°C with a slight vacuum. The heat was sufficient to reduce the viscosity while low enough to avoid initiating the reaction. This combination of reduced viscosity and slight vacuum was found to result in exceptional wetting of the forests. Once bubbling subsided, the vacuum was eliminated, and the temperature was increased to 130°C to cure for 24hrs.

ATR was performed on all samples using a Thermo Scientific Nicolet iS50R FT-IR to identify the completeness of cure, and to observe any potential effects of the presence of CNTs on hydrogen-bonding.

To verify complete wetting of the CNT forests and identify the presence of voids in the PNCs, Micro-CT was performed. A Nikon Metrology (X-Tek) HMXST225 Micro-CT was used to collect Micro-CT images of the PUU PNCs. A voltage of 80 kV and current of 70μA in reflection mode were used with Mo X-ray targets. Reconstructions were performed via VGStudio Max.

2.3 Thermal Characterization

Thermogravimetric analysis (TGA) was done using a TA Instruments Discovery TGA. All tests were run from 23°C to 500°C at a ramp rate of 10°C/min, and pyrolysis occurred in ambient atmosphere.

All differential scanning calorimetry (DSC) data was collected using a TA instruments Discovery DSC. All materials were tested via a heat-cool-heat method, with a temperature range of -100°C to 300°C. Specimens were heated at a rate of 10°C/min.

2.4 Nanoindentation

To achieve the required smoothness, all samples were cryotomed prior to nanoindentation via a Leica Ultracut UCT. The temperature of the cryo-chamber was set to -70°C, significantly below the soft-segment T_g of these materials. Samples were mounted in AFM holders prior to cryotome, which preserved the orientation of the prepared surface through both the cryotoming and nanoindentation processes. This resulted in suitably smooth surfaces for nanoindentation.

It was also important to nanoindent the PUU PNCs in both transverse (PUU211T/PUU541T) and axial (PUU211A/PUU541A) loading configurations, as the anisotropy produced by the alignment of the CNTs is of particular interest. PNCs were sectioned and positioned in the AFM holders such that the CNTs were aligned either parallel or perpendicular to the cryotoming cuts, producing specimens with CNT orientations transversely or axially oriented to the direction of nanoindentation respectively.

A diamond Berkovich tip (R_C ~ 150nm) in a Hysitron TI950 Triboindenter was used to perform quasi-static nanoindentation on the PUU211 and PUU541 materials. The load functions for each material were composed of a 5sec. ramp up, a 5sec. hold, and a 5sec. ramp down. The maximum loads were 200μN for PUU211 materials and 300μN for PUU541 materials, resulting in loading rates of 40μN/sec. and 60μN/sec. respectively. Three locations on the surface of each specimen were selected to perform indentations, with a 4x4 array of indentations spaced at 5μm center-to-center at each location. The result was a total of 48 individual nanoindentations per specimen.

3 RESULTS & DISCUSSION

3.1 PNC Fabrication

To validate the cure process, ATR was run on all samples. Peaks at 2324cm^{-1}, corresponding to unreacted diisocyanate [19], were minuscule in all samples, indicating that 24 hrs. at 130°C is sufficient to cure neat and PNC PUU211 and PUU541. Driving the negligible remaining diisocyanate to complete reaction may be possible, but could require heat which damages the matrix. There was no noticeable difference between the sizes of these peaks in neat and PNC materials, nor between those of PUU211 and PUU541.

Hydrogen-bonding peaks associated with N-H bonds, C-H bonds, and C=O bonds showed no discernible differences associated with the presence of CNTs. All peaks from hydrogen-bonding were less pronounced in the presence of greater hard-segment content, indicative of the fact the hard-segments restrict chain mobility and the aggregation of large phases [20], [21].

Micro-CT images of PUU211-PNC and PUU541-PNC can be found in Figure 1 (a) and (b) respectively. These are top-view images of the samples, with the long axes of the CNTs oriented into the page. These slices are from the center of the specimen, and reveal complete wetting of the CNTs with no voids present.

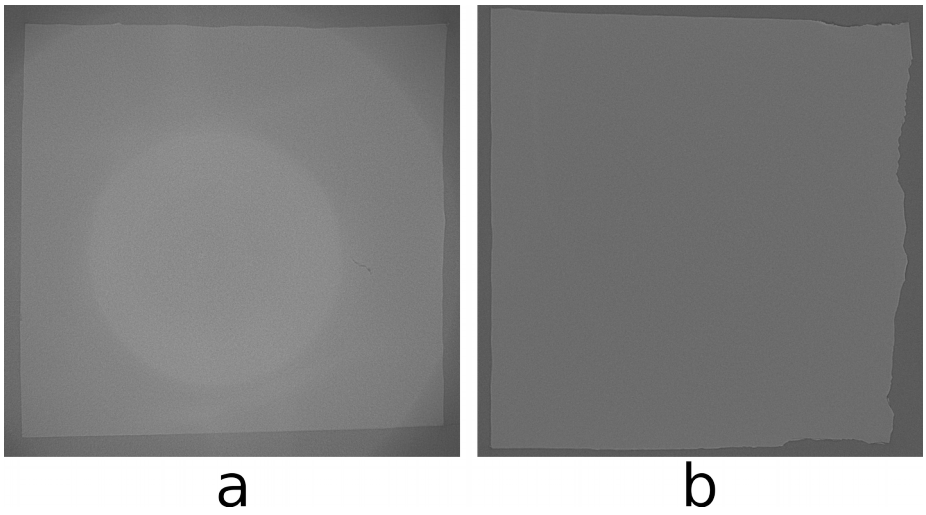

Figure 1: Representative Micro-CT slices of 15mm x 15mm PNCs. (a) PUU 211 (b) PUU541. Notice the absence of voids, confirming complete wetting of the CNT forests.

3.3 TGA

Representative TGA data for PUU211 and PUU541 materials can be found in Figure 2. The dashed lines are the TGA plots, while the solid lines represent the derivative plots. The first thing to notice is that there are two major peaks of thermal degradation; hard-segment degradation is associated with degradation at ~340°C, while soft-segment degradation is associated with ~450°C [22]. The weight percents lost at ~340°C are ~40% and ~66% for PUU211 and PUU541, corresponding with the hard-segment weight compositions of each neat material. The degradations at ~450°C are ~60% and ~34% for PUU211 and PUU541 respectively, corresponding to soft-segment compositions.

The most interesting feature of these plots is perhaps the fact that there is an upward shift in each PUU material due to the presence of the aligned CNTs. This upward shift represents a portion of the hard-segments which have not degraded as they would have in the neat polymers, indicating a degree of thermal stabilization induced by the CNTs. Because this upward shift in weight percent is much greater than the CNT weight percent present in the PNCs, it is clear that the CNTs have enhanced the thermal stability of the materials between the 340°C and 450°C.

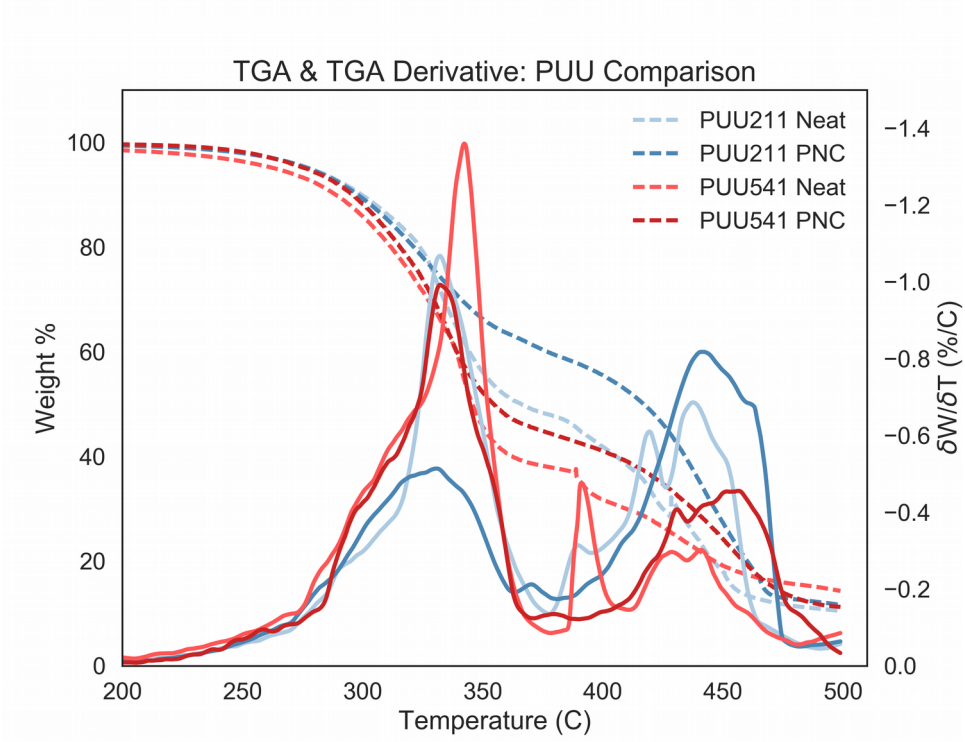

Figure 2: TGA (dashed) and TGA derivative (solid) plots for all PUU materials.

3.4 DSC

First-heat DSC traces for all PUU materials can be found in Figure 3, were endothermic features point upward. The soft-segment T_g, which occurs near -30°C, is noticeably less pronounced in the PUU541 than in the PUU211. This is consistent with the smaller soft-segment composition of the PUU541. The feature at 60°C is associated with short-range hard-segment reordering. The last feature of note is the large exotherm at 250°C, which is significantly more pronounced in the PNCs than in the neat polymers. This indicates that hard-segment crystal formation is thermodynamically favorable in the presence of aligned CNTs at this temperature.

Second-heat DSC traces for all PUU materials can be found in Figure 4, where endothermic features point upward. It is immediately clear that the features from the first heating pass associated with hard-segment rearrangement have disappeared. This is expected since the hard-segment rearrangements are thermodynamically irreversible [23]. Next notice that the soft-segment T_g has dropped from -30°C to -50°C. This is consistent with the phase-separation which has taken place during the annealing step. When the hard-segments crystallized, it allowed the soft-segments to aggregate as well, resulting in a more distinct soft-segment T_g. The phase-separation also results in a soft-segment T_g which is less affected by hard-segment thermal properties, lowering the soft-segment T_g closer to the theoretical temperature [24]. This thermally-induced phase-separation has also permitted soft-segment crystals to form and melt in the PUU211 PNC only. These crystals are found only in the PUU211 and not the PUU541 due to the mobility of the chains from the prevalence of soft-segments in this matrix. Also notice that a distinct soft-segment T_g is almost completely absent from the PUU541 PNC; the combination of high hard-segment composition and the presence of CNTs has restricted mobility to the extent that phase-separation is limited, even with an annealing step. Furthermore, the soft-segment crystals only appear in the PNC because the CNT-induced hard-segment crystallinity leads to a state in which soft-segment aggregation and crystallization are favorable.

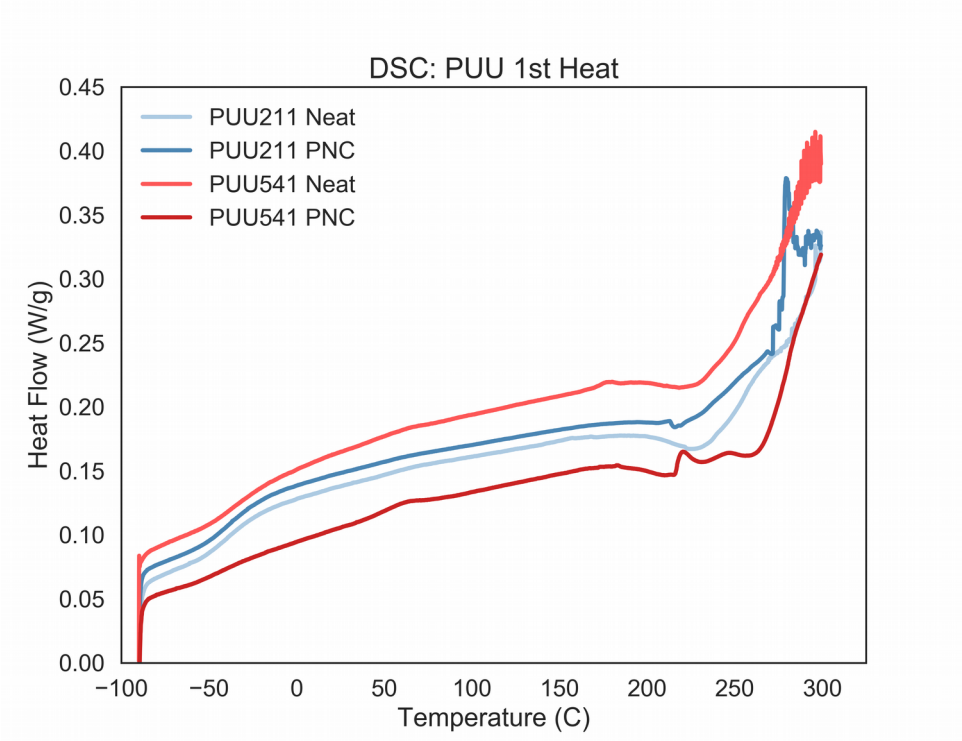

Figure 3: First-heat DSC plots for all PUU materials.

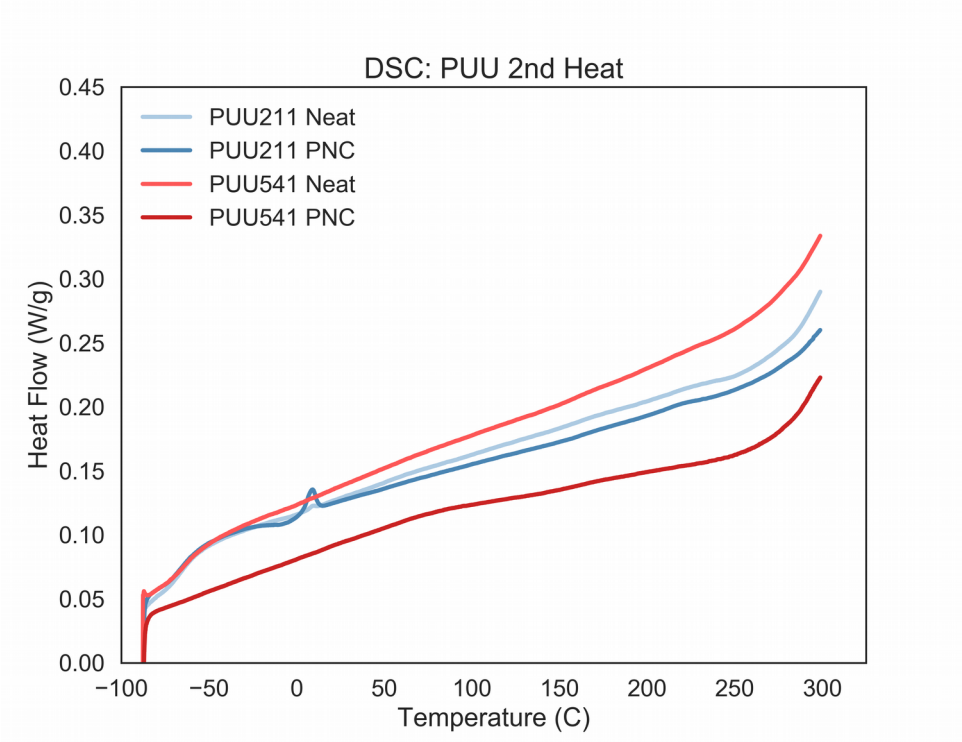

Figure 4: Second-heat DSC plots for all PUU materials.

3.5 Nanoindentation

Characteristic quasi-static nanoindentation curves of PUU211 and PUU541 have been plotted for

comparison purposes in Figure 5. Average quasi-static data for PUU211 and PUU541 materials can also be found below in Table 1. The PUU211N has the lowest indentation modulus of 187MPa, followed by the PUU211T with 277MPa, and then the PUU211A with 849MPa. The fact that the CNT-reinforced PUU211 PNCs have a higher modulus is testament to the reinforcing nature of the CNTs. The mechanism responsible for PUU211T having a lower indentation modulus than the PUU211A is likely related to the columnar compression of the CNTs along their axes. By loading the CNTs in this way, the compressive stiffness of the CNTs is utilized rather than their bending stiffness. Of the PUU541 materials, the PUU541N has the lowest indentation modulus of 1226MPa, followed by the PUU541T with 1319MPa, and then the PUU541A with 1786MPa. These moduli are significantly higher than those recorded for the PUU211 materials, which is to be expected; the PUU541 has a 66% hard phase composition while the PUU211 only has a 40% hard phase composition. Note that the trend continues from the PUU211 specimens in which indentation modulus increases from PUU541N, to PUU541T, to PUU541A.

Another point of interest is the elastic recovery of each material. Note how much lower the elastic recovery is for the PUU211A than that of the other materials (Table 1). A reflection of this can be seen in the unloading curves in Figure 5. Aside from this case, the PUU211N has a much greater elastic recovery than the PUU541N, which is to be expected because of the higher polyol content of the PUU211. Notice that the elastic recovery of the neat polymers and their corresponding PNCs with transverse CNTs have nearly equivalent elastic recoveries. This indicates that a similar mechanism is at play in the loading of each case. Furthermore, the indentation moduli increases are small but measurable when comparing neat and PNCs with transverse CNT, confirming that similar mechanisms are a play during the nanoindentation of each. This is a reasonable conclusion since the matrix material should dominate transverse loading.

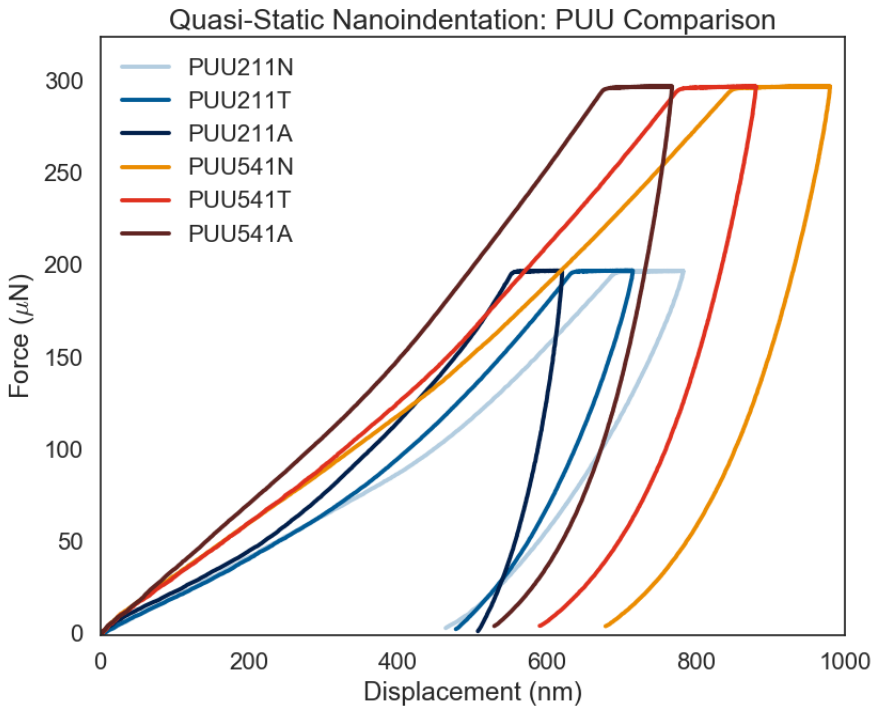

Figure 5: Representative quasi-static nanoindentation curves for each PUU material.

Next consider the PNCs with axial CNTs. The elastic recovery is less in these materials than in their counterparts, though that of the PUU211A is particularly low. PUU211A has an elastic recovery which is ~0.20 times that of PUU211N, while PUU541A has an elastic recovery which is ~0.88 times that of PUU541N. This indicates that a different mechanism is at play during the loading and

unloading of the CNTs when oriented vertically.

Quasi-Static Nanoindentation Summary Data

Material	E_I (MPa)	$\%\Delta E_I$ from Neat	% Recovery
PUU211N	187		38%
PUU211T	277	+48%	34%
PUU211A	849	+354%	7%
PUU541N	1226		19%
PUU541T	1319	+8%	19%
PUU541A	1786	+46%	17%

Table 1: Nomenclature for Neat (N), Transverse (T), and Axial (A) materials, as well as summary data from quasi-static nanoindentation tests.

Table 1 contains a summary of mean data collected via quasi-static nanoindentation: indentation moduli, percent enhancement of PNCs over neat resin, and percent recovery. The enhancement to indentation modulus by the CNTs is profound, particularly in the case of the PUU211. The CNTs offered a 48% improvement to PUU211 indentation modulus in the transverse direction and a 354% improvement in the axial direction. By comparison, the CNTs offered only a 8% enhancement to indentation modulus for PUU541 in the transverse direction and 46% in the axial direction. It is reasonable that the improvement is greater in the softer PUU211 than the PUU541 since there is a greater disparity between the stiffnesses of the CNTs and the matrix. The load is transferred from the softer matrix to the stiffer CNTs to a greater degree because of this mismatch, giving rise to a larger reinforcement of the PUU211. This type of load transfer from lower-modulus materials to higher-modulus fillers is seen in many nanocomposites [25]. Furthermore, the presence of hard-segment crystals aligned and oriented parallel to the axes of the CNTs in the PUU211 and not in the PUU541 could be a major contributor to the greater improvement seen in the PUU211 materials. Nonetheless, in each case, the CNTs oriented axially offered ~6 times more enhancement to indentation modulus than in the transverse direction. This is consistent with the notion that the CNTs contribute more to the loading when orientated axially than transversely. The modulus enhancement is less pronounced in the PUU541 materials because the matrix is much stiffer. As such, the CNTs share more of the load with the matrix material in PUU541, while the CNTs in PUU211A dominate the loading much more.

4 CONCLUSIONS

A novel PUU was developed using a blocked-HMDI which permitted the complete infusion and curing into vertically-aligned CNTs to form PUU PNCs. 24 hrs. at 130°C resulted in completely cured neat and PNC materials, with negligible remaining diisocyanate. Specimens were found to be free of voids thanks to the controlled infusion and curing process.

TGA revealed a hard-segment thermal stabilization in the PNCs relative to the neat materials. From DSC, CNT-induced hard-segment crystallization was observed, which was found to be the cause of the reduced thermal degradation of hard-segments in the PNCs. Hard-segments were found to reduce chain mobility and increase phase-mixing of the polymer. Furthermore, annealing was shown to permit further phase-separation, lowering the soft-segment T_g and accentuating that feature in the DSC. The combination of high hard-segment content and the presence of CNTs prevented this type of phase-separation in the PUU541 PNC by significantly restricting chain mobility.

CNTs were found to reinforce PUU211 to a greater extent than PUU541 due to the stiffness mismatch between the matrix and the CNTs, though larger enhancements to modulus were observed in both cases. Axially oriented CNTs offered a greater enhancement due to the columnar loading of the CNTs, which capitalized on their axial loading rather than transverse bending. The axially-aligned PNCs were clearly more CNT-dominated than the transverse PNCs. The transversely loaded PNCs exhibited greater elastic recovery than the axially loaded materials, and the PUU211 materials had

greater elastic recovery than the PUU541 materials. Both of these observations confirm that the elastic CNTs dominate axial loading and the transversely loaded PNCs are matrix dominated. The greater recover in PUU211 is attributed to the higher soft-segment composition of that matrix material, permitting greater elastic strain.

ACKNOWLEDGMENTS

This project was supported in part by an appointment to the Research Participation Program at the U.S. Army Research Laboratory administered by the Oak Ridge Institute for Science and Education through an interagency agreement between the U.S. Department of Defense and EPA. This work was also supported by Airbux, Embraer, Lockheed Martin, Saab AB, Hexcel, Saertex, TohoTenax, and ANSYS through MIT's Nano-Engineered Composite Aerospace Structures (NECST) Consortium, and was supported in part by the U. S. Army Research Laboratory and the U. S. Army Research Office through the Institute of Soldier Nanotechnologies, under contract number W911NF-13-D-0001. Portions of this work were performed at the Center for Nanoscale Systems (CNS), a member of the National Nanotechnology Infrastructure Network (NNIN), which is supported by the National Science Foundation under NSF award no. ECS-0335765. CNS is part of Harvard University.

REFERENCES

[1] N. Nayak, "Composite materials in aerospace applications," *Int. J. Sci. Res. Publ.*, vol. 4, no. 19, p. 56, 2014.

[2] M. V. Borodii and M. P. Adamchuk, "Life assessment for metallic materials with the use of the strain criterion for low-cycle fatigue," *Int. J. Fatigue*, vol. 31, no. 10, pp. 1579–1587, 2009.

[3] D. P. Davies, S. L. Jenkins, and F. R. Belben, "Survey of fatigue failures in helicopter components and some lessons learnt," *Eng. Fail. Anal.*, vol. 32, pp. 134–151, Sep. 2013.

[4] M. M. Thawre *et al.*, "Effect of ply-drop on fatigue life of a carbon fiber composite under a fighter aircraft spectrum load sequence," *Compos. Struct.*, vol. 127, pp. 260–266, 2015.

[5] D. W. Hoeppner and W. E. Krupp, "Prediction of component life by application of fatigue crack growth knowledge," *Eng. Fract. Mech.*, vol. 6, no. 1, pp. 47–70, 1974.

[6] L. Sheng-Li, Y. Cui, X. Gao, and T. S. Srivatsan, "Influence of exposure to aggressive environment on fatigue behavior of a shot peened high strength aluminum alloy," *Mater. Sci. Eng. A*, vol. 574, pp. 243–252, 2013.

[7] D. W. Hoeppner, *Corrosion Fatigue and Environmentally Assisted Cracking in Aging Military Vehicles*, vol. 323, no. March. 2011.

[8] L. Feng *et al.*, "Compressive and interlaminar shear properties of carbon/carbon composite laminates reinforced with carbon nanotube-grafted carbon fibers produced by injection chemical vapor deposition," *Mater. Sci. Eng. A*, vol. 626, pp. 449–457, 2015.

[9] A. Makeev, "Interlaminar shear fatigue behavior of glass/epoxy and carbon/epoxy composites," *Compos. Sci. Technol.*, vol. 80, pp. 93–100, 2013.

[10] J. H. Koo, *Polymer Nanocomposites*, vol. 53. McGraw-Hill, 2006.

[11] T. L. Wang, C. C. Yu, C. H. Yang, Y. T. Shieh, Y. Z. Tsai, and N. F. Wang, "Preparation, characterization, and properties of polyurethane-grafted multiwalled carbon nanotubes and derived polyurethane nanocomposites," *J. Nanomater.*, vol. 2011, 2011.

[12] F. H. Gojny, M. H. G. Wichmann, U. Köpke, B. Fiedler, and K. Schulte, "Carbon nanotube-reinforced epoxy-composites: Enhanced stiffness and fracture toughness at low nanotube content," *Compos. Sci. Technol.*, vol. 64, no. 15 SPEC. ISS., pp. 2363–2371, 2004.

[13] N. Yamamoto *et al.*, "High-yield growth and morphology control of aligned carbon nanotubes on ceramic fibers for multifunctional enhancement of structural composites," *Carbon N. Y.*, vol. 47, no. 3, pp. 551–560, Mar. 2009.

[14] S. S. Wicks, W. Wang, M. R. Williams, and B. L. Wardle, "Multi-scale interlaminar fracture mechanisms in woven composite laminates reinforced with aligned carbon nanotubes," *Compos. Sci. Technol.*, vol. 100, pp. 128–135, 2014.

[15] B. L. Wardle, D. S. Saito, E. J. García, a. J. Hart, R. Guzmán De Villoria, and E. a. Verploegen, "Fabrication and characterization of ultrahigh-volume-fraction aligned carbon nanotube-polymer composites," *Adv. Mater.*, vol. 20, pp. 2707–2714, 2008.

[16] D. Fragiadakis and J. Runt, "Molecular dynamics of segmented polyurethane copolymers: Influence of soft segment composition," *Macromolecules*, vol. 46, no. 10, pp. 4184–4190, 2013.

[17] S. S. Sarva, S. Deschanel, M. C. Boyce, and W. Chen, "Stress–strain behavior of a polyurea and a polyurethane from low to high strain rates," *Polymer (Guildf).*, vol. 48, no. 8, pp. 2208–2213, Apr. 2007.

[18] S. S. Sarva and A. J. Hsieh, "The effect of microstructure on the rate-dependent stress–strain behavior of poly(urethane urea) elastomers," *Polymer (Guildf).*, vol. 50, no. 13, pp. 3007–3015, Jun. 2009.

[19] A. M. Castagna, A. Pangon, T. Choi, G. P. Dillon, and J. Runt, "The role of soft segment molecular weight on microphase separation and dynamics of bulk polymerized polyureas," *Macromolecules*, vol. 45, no. 20, pp. 8438–8444, 2012.

[20] J. Mattia and P. Painter, "A Comparison of Hydrogen Bonding and Order in a Polyurethane and Poly (urethane - urea) and Their Blends with Poly (ethylene glycol)," *Macromolecules*, vol. 40, pp. 1546–1554, 2007.

[21] J. G. Chavan, S. K. Rath, S. Praveen, S. Kalletla, and M. Patri, "Hydrogen bonding and thermomechanical properties of model polydimethylsiloxane based poly(urethane-urea) copolymers: Effect of hard segment content," *Prog. Org. Coatings*, vol. 90, pp. 350–358, 2014.

[22] J. M. Cervantes-Uc *et al.*, "TGA/FTIR studies of segmented aliphatic polyurethanes and their nanocomposites prepared with commercial montmorillonites," *Polym. Degrad. Stab.*, vol. 94, no. 10, pp. 1666–1677, 2009.

[23] A. M. Castagna, A. Pangon, G. P. Dillon, and J. Runt, "Effect of Thermal History on the Microstructure of a Poly (tetramethylene oxide) -Based Polyurea," 2013.

[24] W. Hu and A. J. Hsieh, "Phase-mixing and molecular dynamics in poly(urethane urea) elastomers by solid-state NMR," *Polymer (Guildf).*, vol. 54, no. 22, pp. 6218–6225, Oct. 2013.

[25] P. M. Ajayan, L. S. Schadler, and P. V Braun, *Nanocomposite Science and Technology*. Wiley-VCH, 2003.